minerals

MDPI

Article

Rheology of Alkali-Activated Mortars: Influence of Particle Size and Nature of Aggregates

Sara Gismera, María del Mar Alonso, Marta Palacios and Francisca Puertas *

Eduardo Torroja Institute for Construction Sciences (IETcc-CSIC), 28033 Madrid, Spain; sgismeradiez@gmail.com (S.G.); mmalonso@ietcc.csic.es (M.d.M.A.); marta.palacios@ietcc.csic.es (M.P.)
* Correspondence: puertasf@ietcc.csic.es

Received: 13 July 2020; Accepted: 15 August 2020; Published: 18 August 2020

Abstract: The effect of two precursors (slag and fly ash), different particle size distribution, and three types of aggregate (siliceous sand, limestone, and recycled concrete) on alkali-activated material (AAM) mortar rheology were studied and compared to their effect on an ordinary Portland Cement (OPC) mortar reference. Stress growth and flow curve tests were conducted to determine plastic viscosity and static and dynamic yield stress of the AAM and OPC mortars. In both OPC and AAM mortars, a reduction of the aggregate size induces a rise of the liquid demand to preserve the plastic consistency of the mortar. In general terms, an increase of the particle size of the siliceous aggregates leads to a decrease of the measured rheological parameters. The AAM mortars require higher liquid/solid ratios than OPC mortars to attain plastic consistency. AAM mortars proved to be more sensitive than OPC mortars to changes in aggregate nature. The partial replacement of the siliceous aggregates with up to 20% of recycled concrete aggregates induced no change in mixing liquid uptake, in either AAM or OPC mortars. All the AAM and OPC mortars studied fitted to the Bingham model.

Keywords: alkali-activated materials; OPC; mortars; rheology; aggregates; slag; fly ash

1. Introduction

Alkali-activated materials (AAMs) are considered eco-efficient and sustainable alternatives to Portland cement (OPC). They are based on the activation of aluminosilicate precursors by highly alkaline solutions. The precursors may be sourced from either industrial waste (such as vitreous blast furnace slag (BFS), coal fly ash (FA)), or used cracking catalysts or natural materials, such as pozzolans or burnt clays [1–4]. AAMs have been shown to owe their mechanical strength and durability to the dense microstructures generated during activation [5–8]. Their performances in those respects vary, however, depending on the aluminosilicate and alkaline activator used and the activation process used to prepare mortars and concretes.

The rheological behavior of such alkali-activated materials differs from that of OPC systems. The key factors determining the rheology of AAM pastes are the precursor nature and the concentration and nature of the activator [9–12]. Although the factors that govern AAM paste rheology have been established, the wide variety of precursors and activation systems renders the accurate prediction of system rheology during on-site placement elusive. Prior optimization studies must be run for nearly every precursor-activator combination. Sodium silicate alkali-activated slag (AAS) system workability and rheology is particularly complex, given the setting and short hardening times involved.

Puertas et al. [9] observed, after only 7 min of reaction, a sharp increase of the shear stress in waterglass-activated slag pastes. However, a breakdown of the structure and decrease of the shear stress occurred when a constant shear rate was applied. The intensity of the signal was enhanced and its time of appearance shortened with the increase of the Na_2O concentration and SiO_2/Na_2O ratio of

the activating solution. These authors justified this phenomenon to the formation of the early reaction products. This effect has also been observed in mortars [13] and concretes [14], and in both cases, the use of longer mixing times led to a better workability. This described phenomenon has not been observed in alkali activated slag pastes with NaOH, KOH, or alkaline carbonates (or even mixtures of all of them). Thus, the determining role of sodium silicate in the rheology of these activated slag systems is clear.

AAM mortars and concrete rheology research is even scarcer where, in addition to the precursor and alkaline activator, consideration must be given to the presence of sand and aggregate morphology and inter-particle friction, as well as the volume fraction occupied by solids in such systems [13–18]. Alonso et al. [15], working with alkali-activated slag, fly ash, and Portland cement mortars, concluded that AAM mortar rheology was more sensitive to changes in the liquid/solid (l/s) and sand/binder ratios than OPC. As noted in the literature, particle size distribution and aggregate nature are determinants in OPC paste, mortar, and concrete rheology [19,20].

It is well known that the particle size of aggregates influences the rheology of mortars and concretes, due to the effect of the packing factor and on the different specific surface of the aggregates [19,21,22]. A smaller size of aggregates leads to a higher demands of mixing liquid in the preparation of their mortars and concretes while preserving their rheological properties. These effects are well known in OPC systems, but much less information is available for AAM systems.

The nature of the aggregates also has a relevant influence on the rheology of OPC systems, mainly due to differences in the morphology of the aggregates that play a key role in the packing factor and possible interactions with cement matrices [23]. Specifically, limestone aggregates generally improve the rheological properties of their OPC mortars and concretes, although their role in the rheology of AAM systems is still largely unknown. Moreover, the total or partial replacement of natural aggregate with recycled construction and demolition waste furthers environmental protection, shrinks the carbon footprint, and ultimately enhances construction industry sustainability. The effect of recycled aggregate on the rheology, mechanical strength, and durability of OPC mortars and concretes has been studied in depth [24–26]. Recycling aggregates contain remaining mortar on their surface that increases the water adsorption [27] and decreases the fluidity of mortars and concrete. Furthermore, recycling aggregates normally have more angular shapes that natural aggregates, leading to lower packing factors than the latter [22,28] The possibility of preparing AAM mortars and concretes with recycled aggregate is of particular interest given the beneficial effect on sustainability. Only a handful of papers have been published on AAM mortars and concretes bearing recycled aggregates, however. Previous research conducted by the authors [29] showed that replacing natural with recycled aggregate by up to 20% has no adverse effect on strength. At the same time, although obviously necessary to understand and use AAM—Recycled aggregate systems and studies on their rheology are practically non-existent.

The research described here consequently aimed to determine the effect of the nature of the sand (siliceous, limestone, or recycle aggregates) on the rheological properties of alkali-activated slag (AAS) and alkali-activated fly ash (AAFA) mortars. Furthermore, the impact of the granulometry of the siliceous sand and its total or partial replacement by limestone and recycle aggregates on the AAS and AAFA mortars rheology has been investigated comparing the findings with the results for OPC mortars.

2. Experimental

2.1. Materials

The alkali-activated mortars studied were AAS, with blast furnace slag (BFS) as the precursor, and AAFA, prepared with coal fly ash (FA), whilst OPC mortars were used as the reference. Table 1 gives the chemical composition of these starting materials determined by XRF in a S8 Tiger Bruker X-ray fluorescence spectrometer. Table 2 shows the particle size distribution determined by laser granulometry and the Blaine specific surface of BFS, FA, and OPC.

The aggregates used were: (i) a siliceous aggregate (S), (ii) a limestone aggregate (L), and (iii) a recycled aggregate (R) from construction and demolition waste. A picture of the three aggregates obtained on a binocular loupe Nikon SMZ-2T with a light supplier Intralux 4000, is shown in Figure 1.

To study the influence of the aggregate granulometry on the rheological parameters of AAM mortars, the siliceous aggregate (S) was sieved to obtain maximum D_{max} values of 2 mm, 1 mm, and 0.5 mm. The percentage distribution by weight of each range used is presented in Table 3. To study of the influence of the nature of the aggregate on the mortar rheology of AAMs, the three aggregates were sieved manually to a maximum diameter of 2 mm and their particle size distributions were equalized to elude possible grain-size effects on the results.

Table 1. Chemical composition of blast furnace slag, fly ash, and OPC.

Material	Component (wt.%)											
	SiO_2	Al_2O_3	Fe_2O_3	MnO	MgO	CaO	Na_2O	K_2O	TiO_2	P_2O_5	SO_3	*LoI
BFS	38.73	11.23	1.09	0.27	8.57	38.56	0.56	0.47	0.40	0.06	1.02	0.00
FA	44.67	24.54	6.85	0.09	1.88	3.88	0.75	3.16	1.04	0.49	1.83	10.72
OPC	21.69	5.88	2.55	0.03	1.56	59.01	0.79	1.24	0.13	0.12	4.15	2.75

*LoI = Loss on ignition at 1000 °C [35].

Table 2. Particle size distribution of blast furnace slag (BFS), fly ash (FA), and cement (OPC).

Precursor/Binder	Dv_{10} (µm)	Dv_{50} (µm)	Dv_{90} (µm)	SSA Blaine (m^2/Kg)
BFS	1.60	10.42	29.81	346
FA	1.53	8.38	35.34	422
OPC	1.71	10.91	33.62	420

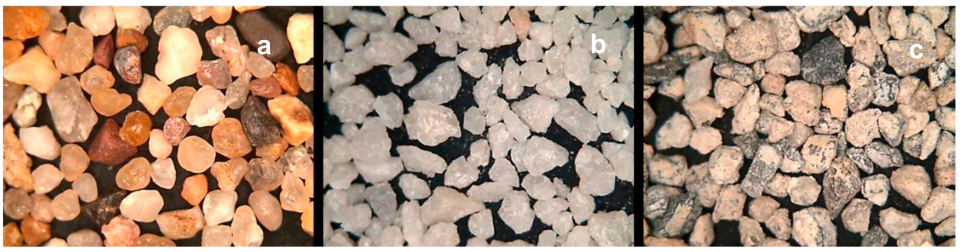

Figure 1. Image of aggregates (**a**) siliceous (S), (**b**) limestone (L), and (**c**) recycled aggregates (R) in fractions of maximum size 1 mm.

Table 3. Particle size distribution of the S aggregate after differential sieving (D_{max} is the maximum diameter of the aggregate).

	% Retained		
Sieve Size mm	D_{max} 2 mm	D_{max} 1 mm	D_{max} 0.5 mm
2.000	-	-	-
1.000	33.47	-	-
0.500	32.64	49.19	-
0.212	13.17	19.79	38.86
0.125	15.48	23.27	45.68
0.063	4.27	6.40	12.66
0.045	0.97	1.40	2.80

Table 4 lists the physical and morphological properties of the siliceous, limestone, and recycled aggregates used. The humidity, water absorption, and density values of S, L, and R aggregates were determined according to EN 1097-6-2014 [30], while the bulk density and percentage of voids were determined according to the EN 1097-3 standard [31] for the different particle size fractions of aggregate S, and for same grain size (as S D_{max} 2 mm) for aggregates L and R. Morphological characterization

(including the aspect, circularity, and convexity values) was determined according to the methodology proposed by Westerholm and Hafid [32,33] and Equations (1) to (3).

$$f - aspect = \frac{D_{min}}{D_{max}} \quad (1)$$

$$f - circularity = \frac{4\pi S}{p^2} \quad (2)$$

$$f - convexity = \frac{p_{Hull}}{p} \quad (3)$$

Moreover, Table 4 lists the mineralogical characterization of different aggregates determined from the Rietveld analysis [34] of the XRD patterns (Bruker AXS D8 Advance X-ray diffractometer).

2.2. Mortar Preparation and Test Conducted

The AAM and OPC mortars were prepared as recommended in EN 196-1 [36] in an Ibertest IB32-040 C2000 mixer. The waterglass solution used to activate the slag (AAS-WG) had a SiO_2/Na_2O ratio of 1.5 and a Na_2O concentration of 4 wt.% (by weight of slag), whilst the AAFA mortars (AAFA-10M) were activated with a 10M NaOH solution and the OPC mortars (OPC) were hydrated with deionized water. The aggregate/binder ratio was 2:1 throughout. All the mortars prepared are described in Table 5.

The following tests were conducted in the different mortars:

- determination of the liquid/solid ratio required for plastic consistency as per the flow table test, determined on the grounds of a 150 ± 10 mm diameter spread pursuant to European standard EN 1015-3:2000 [37];
- determination of fresh state packing density (ϕ) as per Equation (4), and voids content as per Equations (5) and (6) for each mortar [38–40];

where: V is the total volume occupied by the mortar (Equation (7)); vs. is the solids volume; M is the mortar mass; ρ_W is the density of the alkaline solution or water; u_W is the liquid/solid ratio by volume; ρ_α is the cementitious material density; R_α is the volume ratio of the cementitious material to the total solids content; ρ_β is aggregate density; and R_β is the volume ratio of the aggregate to the total solids content;

$$\phi = \frac{V_S}{V} = \frac{1}{1 + voids} \quad (4)$$

$$V_S = \frac{M}{\rho_{w \cdot u_w} + \rho_\alpha \cdot R_\alpha + \rho_\beta \cdot R_\beta} \quad (5)$$

$$Voids\ ratio = \frac{V - V_S}{V_S} \quad (6)$$

$$V = \frac{M}{\rho_{mortar}} = V_S + voids \quad (7)$$

- stress growth test (SGT) conducted on a Viskomat NT mortar rheometer with a blade impeller operating at 1.5 rpm (0.025 s^{-1}) as described in earlier studies [15];
- flow curve test (FCT) run on the same mortars as used for the stress growth test, subsequently subjected to preliminary shear at 30 rpm (0.5 s^{-1}) for 25 s, and then ramped down by 4.5 rpm in 10 s steps, graphing the mean torque at each step against rotational speed and fitting to the respective rheological model to determine the dynamic yield stress and plastic viscosity. Viskomat NT rheometer was calibrated as described in the literature [41] to express the readings in fundamental units.

Table 4. Physical and morphological properties of siliceous (S), limestone (L), and recycled aggregates (R) (D_{max} 2 mm). Quantitative mineralogical composition (wt.%) of S, L, and R aggregates. Quantitative mineralogical composition (wt.%) of S, L, and R aggregates.

Aggregates	Humidity (%)	Water Absorption (%)	Density (g/mL)	Loose Bulk Density (g/mL)	% Voids	f_{aspect}	$f_{sphericity}$	$f_{convexity}$	Quartz	Microcline	Calcite	Dolomite	Moscovite
S	0.07	0.08	2.64	1.68	36.36	0.79	0.82	1.22	98.30	1.70	-	-	-
L	0.02	0.13	2.70	1.69	37.40	0.61	0.72	3.51	-	-	-	100	-
R	0.05	4.81	2.71	1.50	44.65	0.48	0.63	1.83	2.70	-	16.10	79.90	1.30

Table 5. Composition of mortars prepared.

Mortars	Nature of Aggregate	Binder (g)	Liquid (g)	Aggregates (S, L) (g)	Recycled Aggregate (g)
OPC 2 S (D_{max} 2 mm)	100% S	675	351.00	1350	0.00
OPC 1 S (D_{max} 1 mm	100% S	675	357.75	1350	0.00
OPC 0.5 S (D_{max} 0.5 mm)	100% S	675	391.50	1350	0.00
OPC 2 L (D_{max} 2mm)	100% L	675	351.00	1350	0.00
OPC 2 R (D_{max} 2mm)	100% R	675	506.25	0.00	1350
OPC 90% S + 10% R (D_{max} 2 mm)	90% S + 10% R	675	351.00	1215	135
OPC 80% S + 20% R (D_{max} 2 mm)	80% S + 20% R	675	351.00	1080	270
OPC 50% S + 50% R (D_{max} 2 mm)	50% S + 50% R	675	506.25	675	675
AAS-WG 2 S (D_{max} 2 mm)	100% S	675	378.00	1350	0.00
AAS-WG 1 S (D_{max} 1 mm	100% S	675	384.75	1350	0.00
AAS-WG 0.5 S (D_{max} 0.5 mm)	100% S	675	478.75	1350	0.00
AAS-WG 2 L (D_{max} 2 mm)	100% L	675	384.75	1350	0.00
AAS-WG 2 R (D_{max} 2 mm)	100% R	675	513.00	0.00	1350
AAS-WG 90% S + 10% R (D_{max} 2 mm)	90% S + 10% R	675	378.00	1215	135
AAS-WG 80% S + 20% R (D_{max} 2 mm)	80% S + 20% R	675	384.00	1080	270
AAS-WG 50% S + 50% R (D_{max} 2 mm)	50% S + 50% R	675	513.00	675	675
AAFM 2 S (D_{max} 2 mm)	100% S	675	405.00	1350	0.00
AAFM 1 S (D_{max} 1 mm)	100% S	675	418.50	1350	0.00
AAFM 0.5 S (D_{max} 0.5 mm)	100% S	675	479.25	1350	0.00
AAFM 2 L (D_{max} 2 mm)	100% L	675	405.00	1350	0.00
AAFM 2 R (D_{max} 2 mm)	100% R	675	546.75	0.00	1350
AAFM 90% S+10% R (D_{max} 2 mm)	90% S + 10% R	675	405.00	1215	135
AAFM 80% S + 20% R (D_{max} 2 mm)	80% S + 20% R	675	405.00	1080	270
AAFM 50% S + 50% R (D_{max} 2 mm)	50% S + 50% R	675	546.75	675	675

3. Results and Discussion

The variables explored in the preparation of AAM mortars for this study of their rheological behavior were as follows:

(a) The nature of the precursor (BFS, FA) or binder (OPC) activated or hydrated in conditions specific to each as described above;
(b) The particle size distribution of siliceous aggregate (S);
(c) The nature of the aggregates: 100% siliceous (S), 100% limestone (L), or 100% recycled, referred to total aggregate mass. A constant and equal particle size distribution with a maximum diameter of 2 mm and a constant sand/binder ratio of 2/1 were used throughout
(d) S replacement ratio by: 10 wt.%, 20 wt.%, or 50 wt.% of R, likewise referred to total aggregate mass.

The results observed after performing the operations described in the preceding section are discussed below.

3.1. Mortar Liquid/Solid Ratio Required for Plastic Consistency

The liquid/solid ratios required for each mortar to reach European standard EN-1015-3 plastic consistency at 150 ± 10 mm diameter spread are shown in Table 6. In all mortars, and regardless of the precursor or binder used, the smaller the maximum particle diameter of the aggregate, the greater the amount of liquid required to obtain a plastic consistency and, therefore, a certain workability. This effect is due to the increase in the specific surface area with the decrease in the aggregate particle size, which leads to greater liquid demands to moisten the aggregates, as previously described in the literature [42–45]. In particular, the liquid/solid ratio increases 3% when going from D_{max} of 2 mm to 1 mm, while an increase up to 14% has been measured for aggregates of a D_{max} of 0.5 mm.

AAS-WG and AAFA-10M mortars require a higher demand of liquid compared to OPC for the same aggregate granulometries.

Table 6. Fresh state liquid/solid (l/s), spread flow, and density for alkali-activated material (AAM) and OPC mortars with an aggregate/binder ratio of 2/1.

Aggregates	AAS-WG			AAFA-10M			OPC		
Aggregates	l/s	Spread flow (mm)	Density (Kg/m^3)	l/s	Spread Flow (mm)	Density (Kg/m^3)	l/s	Spread Flow (mm)	Density (Kg/m^3)
S D_{max} 2 mm	0.56	151	2242	0.60	151	2184	0.52	150	2192
S D_{max} 1 mm	0.57	155	2195	0.62	149	2174	0.53	152	2181
S D_{max} 0.5 mm	0.65	157	2182	0.71	151	2122	0.58	150	2118
100% S	0.56	151	2242	0.60	151	2184	0.52	150	2192
100% L	0.57	155	2189	0.60	148	2162	0.52	148	2180
100% R	0.76	155	2032	0.81	147	1975	0.75	155	2018
90% S + 10% R	0.57	158	2239	0.61	147	2176	0.53	147	2189
80% S + 20% R	0.57	150	2216	0.62	144	2119	0.54	146	2159
50% S + 50% R	0.65	151	2183	0.73	151	2064	0.64	157	2124

Table 6 shows that where siliceous or limestone aggregate was used the liquid/solid ratios were practically the same for the AAS-WG, AAFA-10, and OPC mortars. A closer analysis revealed that the liquid/solid ratio for both aggregate types was 0.56 in AAS-WG mortars, 0.60 for AAFA-10M mortars, and 0.52 in the OPC materials. In other words, the AAM mortars required more liquid to attain the same spread as OPC. That may be attributable to the greater density of the waterglass and 10M NaOH activators (around 1.27 g/cm^3). An earlier paper [15] reported the need for a higher liquid/solid ratio in AAFA-10M mortars and the generally greater AAM mortar sensitivity to change in liquid/solid ratios.

As expected, when 100% recycled aggregate was used, the liquid/solid ratio needed, was 25% to 30% higher. At 4.81%, water absorption was much higher in R (Table 4) than in aggregates S (0.08%) or L (0.13%), because the mortar adhered to the recycled aggregate particles rendered a higher specific surface area, consequently raising mixing water uptake [46]. Replacing S with up to 20% R (Table 6) led to no change in water demand, with values nearly identical to those found with 100% siliceous aggregate in both AAM and OPC mortars. At a replacement ratio of 50%, however, the liquid/solid ratio rose by a substantial 16% to 23% in all three mortars, with the greatest increase in AAFA-10M due to the added effect of the higher density of the activating solution, as noted earlier. In short, the AAM mortars, particularly AAFA-10M, required somewhat higher liquid/solid ratios than OPC mortars to attain a plastic consistency, whereas the partial replacement of S with up to 20% R induced no change in mixing liquid uptake in either the AAM or the OPC mortars.

Packing density (φ) calculated with Equation (4) and voids content with Equation (6) are given in Table 7 for each mortar. The effect of aggregate type on packing density in OPC mortars and concretes has been firmly established [47–50]. The analogous effect on AAM mortars has not been studied to date, however. Since in this study plastic consistency was defined as one of the parameters for mortar analysis, the l/s ratio was explored, given its relevance to the subsequent analysis of packing density and voids content.

The data in Table 7 attest to a number of effects:

(a) With the maximum particle size (D_{max} 2 mm), the packing density is slightly higher due to the greater particle size distribution, allowing particles of different sizes to present better compaction. This effect appears to be somewhat more pronounced in AAFA mortars. Therefore, the higher the packing density, the lower the void content and the greater the amount of available paste to lubricate the mortar [51–53]. This effect has been observed in both OPC and AAM mortars;

(b) Generally speaking, and irrespective of the size and nature of the aggregate, AAM mortars had slightly higher packing densities than the OPC reference. A possible explanation for those findings may lie in the physical characteristics of the activator solutions (higher density and

viscosity) and to a lesser extent in the surface characteristics of the precursors (the vitreous slag in particular);

(c) Replacing siliceous with limestone aggregate always entailed a decline in packing density and a rise in the voids content in the mortars studied. The same observation was made by authors researching OPC concretes [47,49,54] and has been attributed to the fact that limestone aggregate is crushed, generating uneven particles with sharp edges (see morphological factors Table 4) that hinder compact packing and favor the formation of inter-particle voids;

(d) The partial replacement of siliceous with recycled aggregate in AAM and OPC mortars apparently slightly lowered packing density and raised the voids content. Further to Table 7, at 20% replacement the voids values were quite similar to those observed for 100% siliceous aggregate-bearing mortar in AAM and OPC mortars both.

The foregoing confirmed that the size and nature of the aggregate affects mortar packing density and voids content, slightly more in Waterglass-AAS than in NaOH-AAFA and OPC mortars. Mortars bearing L aggregates showed a slightly lower packing density than mortars prepared with S aggregates. The same albeit less intense effect was observed in the mortars with recycled concrete aggregate.

Table 7. Packing density (ϕ) and voids ratio in AAS-WG, AAFA-10M, and OPC mortars by aggregate size and type.

Aggregates	AAS WG		AAFA 10M		OPC	
	ϕ	Voids Ratio	ϕ	Voids Ratio	ϕ	Voids Ratio
S D_{max} 2 mm	0.69	0.44	0.71	0.41	0.67	0.48
S D_{max} 1 mm	0.68	0.47	0.70	0.42	0.67	0.49
S D_{max} 0.5 mm	0.67	0.50	0.58	0.48	0.65	0.54
100% S	0.69	0.44	0.71	0.41	0.67	0.48
100% L	0.66	0.51	0.70	0.44	0.66	0.52
100% R	0.68	0.47	0.70	0.45	0.67	0.50
90% S + 10% R	0.70	0.43	0.71	0.40	0.68	0.47
80% S + 20% R	0.70	0.43	0.70	0.43	0.67	0.48
50% S + 50% R	0.70	0.43	0.69	0.45	0.67	0.49

3.2. Mortar Rheological Parameters

Table 8 show the static (τ_{static}) and dynamic ($\tau_{dynamic}$) yield stress and plastic viscosity (μ) for all the mortars studied. The τ_{static} values calculated from the stress growth test (SGT) findings were converted to the International System of Units. Plastic viscosity (μ) was found as the slope of the linear regression line and dynamic shear as the y-intercept for the Bingham equation (Equation (8)) calculated from the flow curve test (FCT) data (see Figures 2–4).

$$\tau = \tau_0 + \mu \cdot \dot{\gamma} \quad (8)$$

The conclusion to be drawn from the FCT data in Figures 2–4 is that all the mortars studied here behaved as Bingham fluids.

The values for the three rheological parameters listed in Table 8 for the AAM and OPC mortars prepared with siliceous aggregate with different particle sizes and the various aggregates are indicative of the following:

(a) Irrespective of particle size or nature aggregate used, the AAS-WG mortars had consistently lower τ_{static} and $\tau_{dynamic}$ values than the AAFA-10M and OPC materials. The inference is that such mortars call for less energy to begin to flow. Similar findings reported for AAS paste [15] have been associated essentially with the fluidizing characteristics of the waterglass activator. The AAS-WG mortars also exhibited the greatest plastic viscosity as a result of the high viscosity of the activator;

(b) The highest τ_{static} and $\tau_{dynamic}$ values were found for the OPC mortars followed by the AAFA-10M materials, with the former exhibiting the lowest plastic viscosity. These observations are attributable to inter-particle interaction, especially in OPC mortars, and low initial binder reactivity in the AAFA-10M mortars;

(c) Regardless of the precursor or binder used, rheological parameters increase when the maximum particle size decreases. This effect is mainly due to several reasons: i) the lower the D_{max}, the higher surface area of the aggregates, which leads to an increase in the friction between the particles and the yield stress [32,53]. ii) As the surface area of the aggregates increases, the adsorption of liquid rises, leaving less water available for the paste to lubricate the aggregates, and iii) the smaller the maximum particle diameter of the aggregate has a lower grain size distribution that leads to a packing density [44,47,54] and higher volume of intergranular voids (See Table 7);

(d) In both the AAM and OPC mortars replacing siliceous with limestone and recycled aggregate entailed rises in τ_{static} and $\tau_{dynamic}$, a logical outcome inasmuch as siliceous aggregate particles are more spherical and limestone and recycled aggregates are more uneven (see the sphericity and convexity factor data in Table 3);

(e) Incrementally replacing siliceous by recycled aggregates from 10% to 100% also induced (practically linear) rises in τ_{static} and $\tau_{dynamic}$.

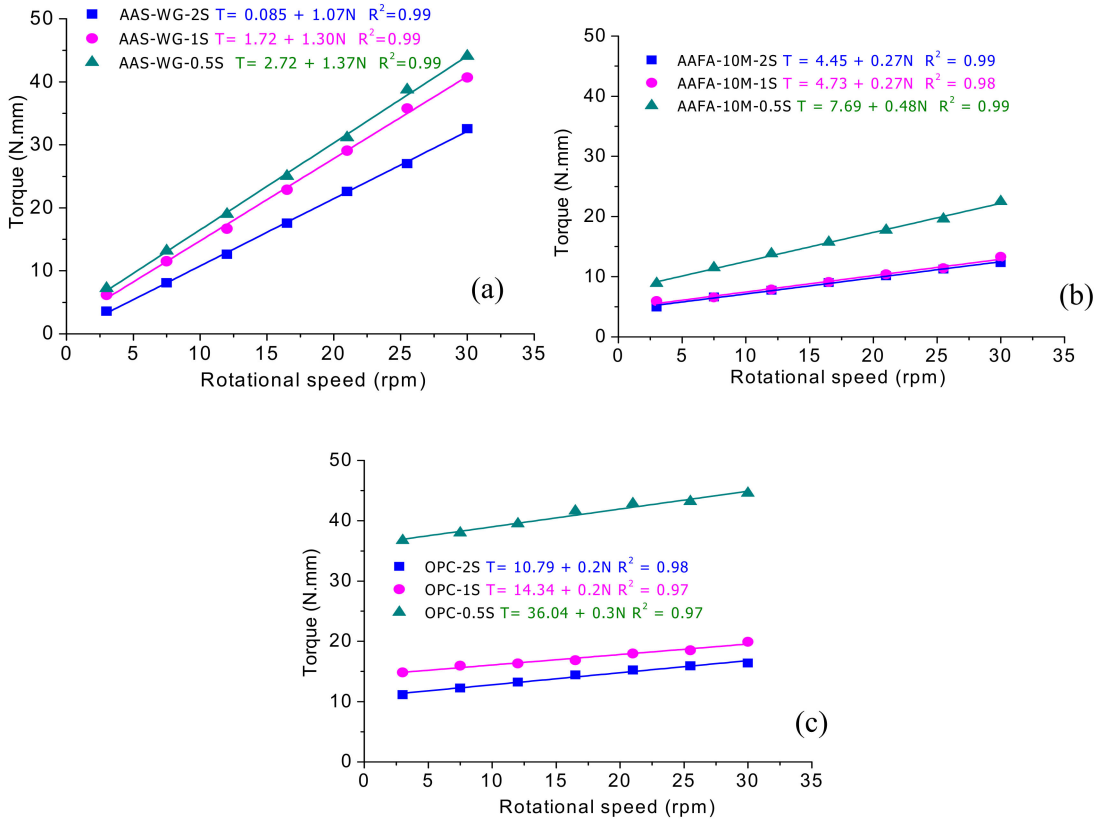

Figure 2. Flow curves for: (**a**) AAS-WG, (**b**) AAFA-10M, and (**c**) OPC with different particle size of siliceous, aggregate (D_{max} = 2 mm (2S), D_{max} 1 mm (1S), and D_{max} 0.5 mm (0.5S)).

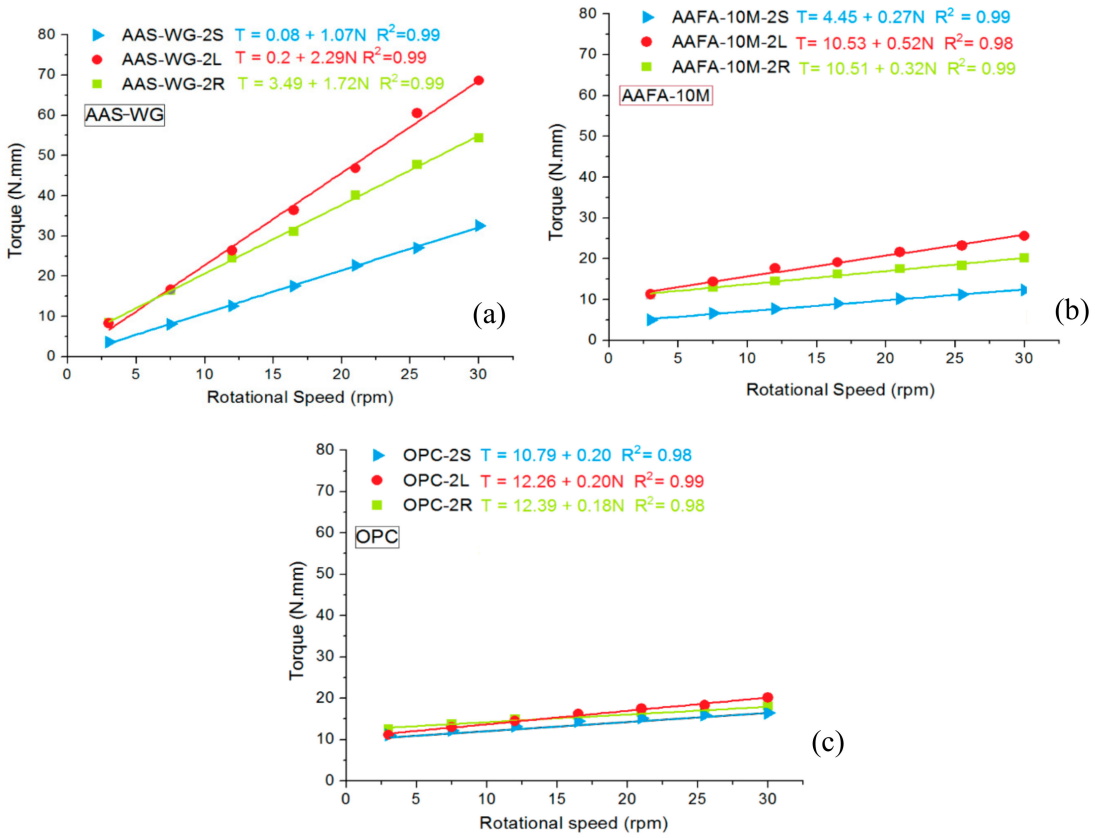

Figure 3. Flow curves for: (**a**) AAS-WG, (**b**) AAFA-10M, and (**c**) OPC with siliceous (2S), limestone (2L) or recycled (2R) aggregate and identical particle size distributions with D_{max} = 2 mm.

Table 8. Static (τ_{static}) and dynamic ($\tau_{dynamic}$) yield stress and μ in fundamental units for the mortars studied, bearing siliceous, limestone, or recycled aggregate.

Aggregates	**AAS WG**			**AAFA 10M**			**OPC**		
Aggregates	**τ_{static} (Pa)**	**$\tau_{dynamic}$ (Pa)**	**μ (Pa·s)**	**τ_{static} (Pa)**	**$\tau_{dynamic}$ (Pa)**	**μ (Pa·s)**	**τ_{static} (Pa)**	**$\tau_{dynamic}$ (Pa)**	**μ (Pa·s)**
S D_{max} 2 mm	28.4	0.7	26.2	51.0	40.2	6.6	120.0	97.4	4.9
S D_{max} 1 mm	50.3	15.5	32.0	57.9	42.67	6.9	122.3	129.4	4.7
S D_{max} 0.5 mm	153.5	24.5	33.7	103.5	69.4	11.7	337.6	325.2	7.1
100% S	28.4	0.7	26.2	51.0	40.2	6.6	120.0	97.4	4.9
100% L	62.5	1.8	56.0	106.6	95.0	12.7	142.8	110.6	4.9
100% R	75.8	31.5	42.0	127.0	94.8	7.8	225.0	111.8	4.4
90% S + 10% R	38.2	15.9	26.7	59.6	49.2	7.3	124.0	99.9	4.9
80% S + 20% R	48.3	27.6	39.9	76.4	64.4	9.5	123.1	101.0	4.9
50% S + 50% R	54.8	30.4	40.8	86.2	73.5	9.29	174.6	109.5	4.7

The effect of the nature of the aggregate on τ_{static}, $\tau_{dynamic}$ and μ in these mortars was analyzed more exhaustively by comparing (in Figure 5) the values found for the AAM and OPC mortars with L and R aggregates to the values for the mortars bearing S aggregate.

As the Figure 5 shows, the AAM mortars were more sensitive to replacing siliceous with limestone or recycled aggregates than the OPC materials, for the three rheological parameters analyzed rose more steeply in the former, in particular in AAS-WG.

The extent of the effect of changing the type of aggregate varied depending on the parameter. The greatest variation in τ_{static} was observed in the recycled aggregates followed by the limestone aggregates-bearing mortars. The rise in τ_{static} in the limestone aggregate mortars was attributable to the high convexity factor found for L (f-convexity = 3.51; see Table 4), which induced greater friction

between the particles, hindering initial mortar flow. In aggregate R, the effect on τ_{static} was the result of the combination of two factors, the sharper edges in R than in S (see Table 4) and its rougher texture due to the mortar adhered to the surface, which increased inter-particle friction.

The widest variation in the $\tau_{dynamic}$ values was induced by recycled aggregate in all the mortars. The inference, again, is that aggregate texture was the most significant factor once the mortar started to flow, i.e., in a state not beginning at rest. That finding was especially visible in the AAS-WG mortars, where the effect was heightened by the angular morphology of slag particles that have been shown to flocculate at early reaction times [9].

Irrespective of the precursor, the mortars with siliceous aggregate exhibited the lowest plastic viscosity (μ) values, for the greater particle sphericity induces greater packing, lower inter-particle friction, and lesser plastic viscosity [33,55]. The μ values barely varied with changes in aggregate in the OPC mortars. The effect of the change in aggregate type on AAFA-10M mortar viscosity was of scant significance, for FA activation reactions do not take place at ambient temperature [11], whereas wider differences were observed in μ in the AAS-WG mortars due to flocculation, as reported in earlier studies [9,13]. Longer mixing times in waterglass-activated slag have been shown [14,56] to improve mortar and concrete workability, lessening the adverse effect of such initial flocculation.

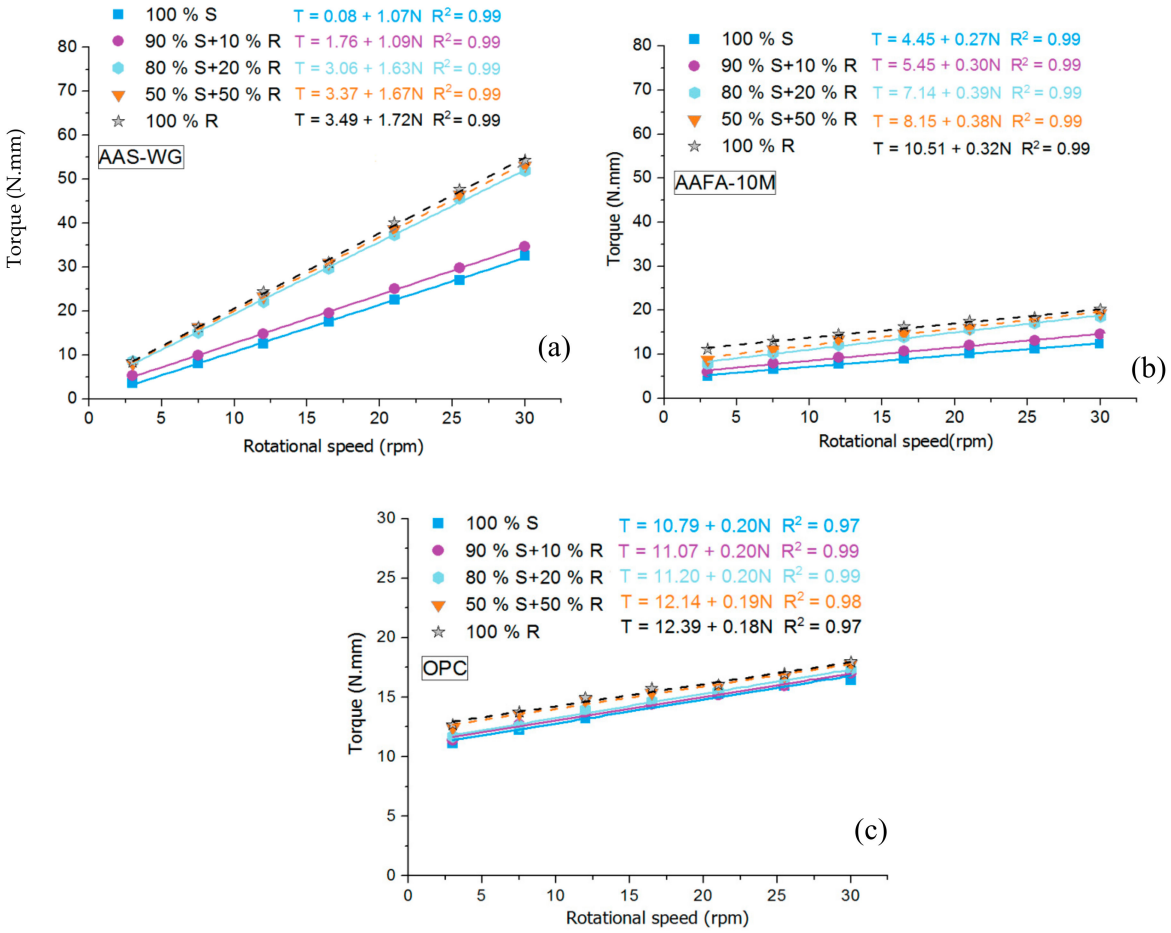

Figure 4. Flow curves for: (**a**) AAS-WG; (**b**) AAFA-10M; and (**c**) OPC with different replacement ratios (S with R).

The effect of replacing siliceous aggregate with recycled aggregate on the rheological parameters intensified with rising replacement ratios, as expected (Figure 5). Rates of up to 10% induced no significant change in τ_{static} or μ in any of the mortars except AAS-WG.

This study showed, in short, that the rheological parameters of AAM and particularly AAS-WG mortars undergo very significant rises when limestone aggregates or especially recycled aggregates are used instead of siliceous aggregate. These effects are much less accentuated in AAFA-10M mortars.

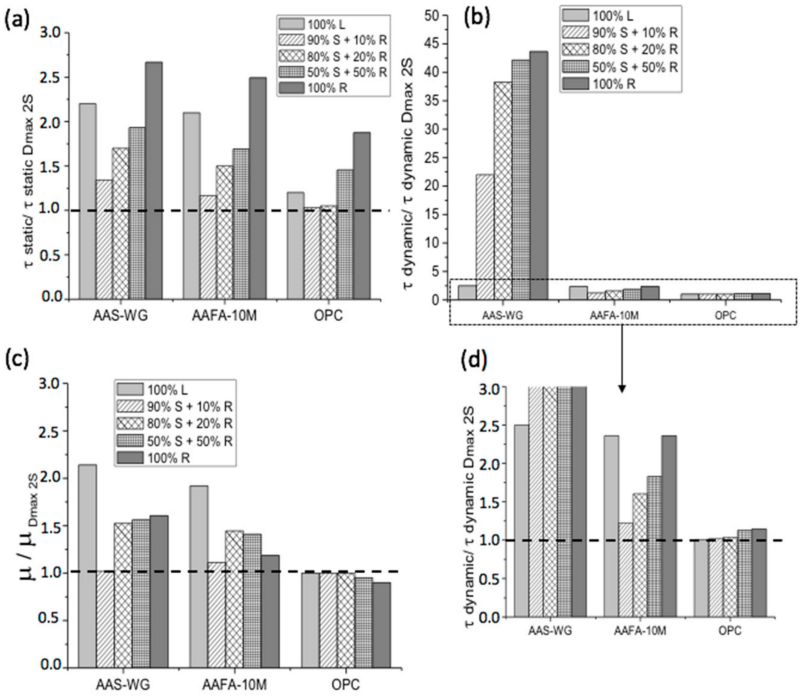

Figure 5. Variation in (**a**) static (τ_{static}) and (**b**,**d**) dynamic ($\tau_{dynamic}$) shear, and (**c**) plastic viscosity (μ), when siliceous (S) aggregate was replaced with 100% limestone (L), or different percentages of recycled (R) aggregate. Values have been normalized with respect to the mortars with 100% siliceous aggregate and a D_{max} = 2 mm.

4. Conclusions

The conclusions drawn from the present findings are discussed below:

(a) In both OPC and AAM mortars, the smaller the aggregate size, the higher the liquid/solid ratio required to achieve a similar plastic consistency. Plastic viscosity as well as static and dynamic yield stress increase with the decrease in maximum particle size. This effect is due to the increase of the interparticle friction and the decrease of the packing density of the mortars due to the narrower size distribution of the aggregate with the smaller size (D_{max} = 0.5);

(b) The AAM mortars, particularly the AAFA-10M materials, required higher liquid/solid ratios than OPC mortars to attain plastic consistency, whereas the partial replacement of the siliceous aggregate with up to 20% of recycled aggregate induced no change in in mixing liquid uptake in either AAM or OPC mortars;

(c) Aggregate nature affected mortar packing density and voids content slightly more intensely in waterglass-AAS mortars than in NaOH-AAFA and OPC mortars. Possibly the most visible effect was found for mortars prepared with limestone aggregate, which, under all the conditions studied, exhibited lower packing density and a higher voids content than siliceous aggregate-containing mortars, due to the uneven shape of limestone aggregate particles. Although less accentuated, the same effect was observed in the mortars with recycled concrete aggregate;

(d) All of the AAS-WG, AAFA-10M, and OPC mortars studied conformed well to the Bingham plastic model;

(e) AAM mortars were found to be more sensitive than OPC mortars to changes in aggregate nature. For as a rule, the values of the three rheological parameters studied (τ_{static}, $\tau_{dynamic}$ and μ) rose

more substantially in the former and, consistently, more steeply in AAS-WG mortars when siliceous aggregate was replaced with recycled concrete or limestone aggregates. Aggregate texture and surface properties played an instrumental role in parameters τ_{static} and $\tau_{dynamic}$ in all the mortars, an effect especially visible when the mortars with limestone and recycled concrete aggregates were compared to the siliceous aggregate-bearing materials. The values of the three rheological parameters rose with rising replacement ratio (when recycled aggregates was substituted for siliceous one) in the AAM mortars, particularly AAS-WG. Rates of up to 10% induced no significant change in τ_{static} or μ in any of the mortars except AAS-WG.

Author Contributions: Conceptualization, F.P. and M.d.M.A.; methodology, S.G.; formal analysis, F.P., M.d.M.A., M.P., S.G.; writing—original draft preparation, F.P., M.d.M.A.; writing—review and editing, F.P., M.d.M.A. M.P. S.G.; supervision, F.P., M.d.M.A., M.P.; project administration, F.P.; funding acquisition, F.P. All authors have read and agreed to the published version of the manuscript.

Funding: This study was funded by AEI-/FEDER/UE under projects BIA2013-47876-C2-1-P and BIA2016-77252-P. Marta Palacios thanks Consejería de Educación e Investigación (Comunidad de Madrid) for funding the 2016-T1/AMB-1434 project in the frame of "Ayudas de Atracción de Talento Investigador" and MCIU/AEI/FEDER, UE for funding the RTI2018-099326-A-I00 project.

Conflicts of Interest: The authors declare that there is not conflict of interest.

References

1. Palomo, A.; Krivenko, P.; Garcia-Lodeiro, I.; Kavalerova, E.; Maltseva, O.; Fernández-Jiménez, A. A review on alkaline activation: New analytical perspectives. *Mater. Constr.* **2014**, *64*, e022. [CrossRef]
2. Provis, J.L. Alkali-activated materials. *Cem. Concr. Res.* **2018**, *114*, 40–48. [CrossRef]
3. Robayo-Salazar, R.A.; De Gutiérrez, R.M.; Puertas, F. Alkali-activated binary concrete based on a natural pozzolan: Physical, mechanical and microstructural characterization. *Mater. Constr.* **2019**, *69*, 191. [CrossRef]
4. Pacheco-Torgal, F.; Labrincha, J.A.; Leonelli, C.; Palomo, A.; Chindaprasirt, P. *Handbook of Alkali-Activated Cements, Mortars and Concretes*; Series in Civil and Structural Engineering; Woodhead Publishing: Cambridge, UK, 2015. [CrossRef]
5. Singh, N.B. Fly Ash-Based Geopolymer Binder: A Future Construction Material. *Minerals* **2018**, *8*, 299. [CrossRef]
6. Provis, J.L.; Palomo, A.; Shi, C. Advances in understanding alkali-activated materials. *Cem. Concr. Res.* **2015**, *78*, 110–125. [CrossRef]
7. Varga, C.; Alonso, M.D.M.; De Gutiérrez, R.M.; Mejía, J.; Puertas, F. Decalcification of alkali-activated slag pastes. Effect of the chemical composition of the slag. *Mater. Struct.* **2014**, *48*, 541–555. [CrossRef]
8. Fernández-Jiménez, A.; Palomo, J.; Puertas, F. Alkali-activated slag mortars. *Cem. Concr. Res.* **1999**, *29*, 1313–1321. [CrossRef]
9. Puertas, F.; Varga, C.; Alonso, M.D.M. Rheology of alkali-activated slag pastes. Effect of the nature and concentration of the activating solution. *Cem. Concr. Compos.* **2014**, *53*, 279–288. [CrossRef]
10. Kashani, A.; Provis, J.L.; Qiao, G.G.; Van Deventer, J.S. The interrelationship between surface chemistry and rheology in alkali activated slag paste. *Constr. Build. Mater.* **2014**, *65*, 583–591. [CrossRef]
11. Palacios, M.; Alonso, M.D.M.; Varga, C.; Puertas, F. Influence of the alkaline solution and temperature on the rheology and reactivity of alkali-activated fly ash pastes. *Cem. Concr. Compos.* **2019**, *95*, 277–284. [CrossRef]
12. Xiang, J.; Liu, L.-P.; Cui, X.-M.; He, Y.; Zheng, G.; Shi, C. Effect of limestone on rheological, shrinkage and mechanical properties of alkali—Activated slag/fly ash grouting materials. *Constr. Build. Mater.* **2018**, *191*, 1285–1292. [CrossRef]
13. Palacios, M.; Banfill, P.; Puertas, F. Rheology and Setting of Alkali-Activated Slag Pastes and Mortars: Effect of Organic Admixture. *ACI Mater. J.* **2008**, *105*, 140–148. [CrossRef]
14. Puertas, F.; González-Fonteboa, B.; González-Taboada, I.; Alonso, M.D.M.; Torres-Carrasco, M.; Rojo, G.; Martínez-Abella, F. Alkali-activated slag concrete: Fresh and hardened behaviour. *Cem. Concr. Compos.* **2018**, *85*, 22–31. [CrossRef]
15. Alonso, M.D.M.; Gismera, S.; Blanco, M.; Lanzón, M.; Puertas, F. Alkali-activated mortars: Workability and rheological behaviour. *Constr. Build. Mater.* **2017**, *145*, 576–587. [CrossRef]

16. You, N.; Liu, Y.; Gu, D.; Ozbakkaloglu, T.; Pan, J.; Zhang, Y. Rheology, shrinkage and pore structure of alkali-activated slag-fly ash mortar incorporating copper slag as fine aggregate. *Constr. Build. Mater.* **2020**, *242*, 118029. [CrossRef]
17. Wetzel, A.; Middendorf, B. Influence of silica fume on properties of fresh and hardened ultra-high performance concrete based on alkali-activated slag. *Cem. Concr. Compos.* **2019**, *100*, 53–59. [CrossRef]
18. Kamani, M.; Ajalloeian, R. The effect of rock crusher and rock type on the aggregate shape. *Constr. Build. Mater.* **2020**, *230*. [CrossRef]
19. Krieger, I.M.; Dougherty, T.J. A Mechanism for Non-Newtonian Flow in Suspensions of Rigid Spheres. *Trans. Soc. Rheol.* **1959**, *3*, 137–152. [CrossRef]
20. Yahia, A.; Mantellato, S.; Flatt, R.J. Concrete rheology: A basis for understanding chemical admixtures. In *Science and Technology of Concrete Admixtures*; Elsevier BV: Woodhead Publishing (an imprint of Elsevier): Cambridge, UK, 2016; pp. 97–127.
21. Wills, M.H., Jr. How aggregate particle shape influences concrete mixing water requirement and strength. *J. Mat.* **1967**, *2*, 843–865.
22. Cepuritis, R.; Jacobsen, S.; Pedersen, B.; Mørtsell, E. Crushed sand in concrete—Effect of particle shape in different fractions and filler properties on rheology. *Cem. Concr. Compos.* **2016**, *71*, 26–41. [CrossRef]
23. Mehdipour, I.; Khayat, K.H. Understanding the role of particle packing characteristics in rheo-physical properties of cementitious suspensions: A literature review. *Constr. Build. Mater.* **2018**, *161*, 340–353. [CrossRef]
24. Kurda, R.; De Brito, J.; Silvestre, J. Influence of recycled aggregates and high contents of fly ash on concrete fresh properties. *Cem. Concr. Compos.* **2017**, *84*, 198–213. [CrossRef]
25. Lavado, J.; Bogas, J.; De Brito, J.; Hawreen, A. Fresh properties of recycled aggregate concrete. *Constr. Build. Mater.* **2020**, *233*, 117322. [CrossRef]
26. Carro-López, D.; González-Fonteboa, B.; De Brito, J.; Martínez-Abella, F.; Taboada, I.G.; Da Silva, P.R. Study of the rheology of self-compacting concrete with fine recycled concrete aggregates. *Constr. Build. Mater.* **2015**, *96*, 491–501. [CrossRef]
27. Sánchez-Roldán, Z.; Valverde-Palacios, I.; Valverde-Espinosa, I.; Martín-Morales, M. Microstructural analysis of concretes manufactured with recycled coarse aggregates pre-soaked using different methods. *Mater. Constr.* **2020**, *70*, 228. [CrossRef]
28. Ferraris, C.F.; De Larrard, F. Testing and modelling of fresh concrete rheology. *Natl. Inst. Stand. Technol. Interag. Rep.* **1998**, 6094. [CrossRef]
29. Alonso, M.D.M.; Rodríguez, A.; Puertas, F. Viability of the use of construction and demolition waste aggregates in alkali-activated mortars. *Mater. Constr.* **2018**, *68*, 164. [CrossRef]
30. EN 1097-6. *Tests for Mechanical and Physical Properties of Aggregates—Part 6: Determination of Particle Density and Water Absorption*; Comite Europeen de Normalisation: Brussels, Belgium, 2013.
31. EN 1097-3. *Tests for Mechanical and Physical Properties of Aggregates—Part 3: Determination of Loose Bulk Density and Voids*; Comite Europeen de Normalisation: Brussels, Belgium, 1999.
32. Westerholm, M.; Lagerblad, B.; Silfwerbrand, J.; Forssberg, E. Influence of fine aggregate characteristics on the rheological properties of mortars. *Cem. Concr. Compos.* **2008**, *30*, 274–282. [CrossRef]
33. Hafid, H.; Ovarlez, G.; Toussaint, F.; Jezequel, P.; Roussel, N. Effect of particle morphological parameters on sand grains packing properties and rheology of model mortars. *Cem. Concr. Res.* **2016**, *80*, 44–51. [CrossRef]
34. Rietveld, H.M. A profile refinement method for nuclear and magnetic structures. *J. Appl. Crystallogr.* **1969**, *2*, 65–71. [CrossRef]
35. UNE-EN. *UNE-EN 196-2 Method of Testing Cement—Part 2: Chemical Analysis*; Comite Europeen de Normalisation: Brussels, Belgium, 2014.
36. EN 196-1. *Methods of Testing Cement—Part 1: Determination of Strength*; Comite Europeen de Normalisation: Brussels, Belgium, 2018.
37. UNE-EN-1015-3. *Methods of Test for Mortar for Masonry. Part 3: Determination of Consistence of Fresh Mortar (by Flow Table)*; Comite Europeen de Normalisation: Brussels, Belgium, 2000.
38. Wong, H.H.C.; Kwan, A.K.H. Packing density of cementitious materials: Part 1—Measurement using a wet packing method. *Mater. Struct.* **2007**, *41*, 689–701. [CrossRef]
39. Kwan, A.; Fung, W. Packing density measurement and modelling of fine aggregate and mortar. *Cem. Concr. Compos.* **2009**, *31*, 349–357. [CrossRef]

40. Diederich, P.; Mouret, M.; De Ryck, A.; Ponchon, F.; Escadeillas, G. The nature of limestone filler and self-consolidating feasibility—Relationships between physical, chemical and mineralogical properties of fillers and the flow at different states, from powder to cement-based suspension. *Powder Technol.* **2012**, *218*, 90–101. [CrossRef]
41. Flatt, R.J.; LaRosa, D.; Roussel, N. Linking yield stress measurements: Spread test versus Viskomat. *Cem. Concr. Res.* **2006**, *36*, 99–109. [CrossRef]
42. Reddy, B.V.; Gupta, A. Influence of sand grading on the characteristics of mortars and soil–cement block masonry. *Constr. Build. Mater.* **2008**, *22*, 1614–1623. [CrossRef]
43. Lim, S.K.; Tan, C.S.; Chen, K.P.; Lee, M.L.; Lee, W.P. Effect of different sand grading on strength properties of cement grout. *Constr. Build. Mater.* **2013**, *38*, 348–355. [CrossRef]
44. Harini, M.; Shaalini, G.; Dhinakaran, G. Effect of size and type of fine aggregates on flowability of mortar. *KSCE J. Civ. Eng.* **2011**, *16*, 163–168. [CrossRef]
45. Haach, V.G.; Vasconcelos, G.; Lourenço, P. Influence of aggregates grading and water/cement ratio in workability and hardened properties of mortars. *Constr. Build. Mater.* **2011**, *25*, 2980–2987. [CrossRef]
46. Neno, C.; De Brito, J.; Veiga, R. Using fine recycled concrete aggregate for mortar production. *Mater. Res.* **2013**, *17*, 168–177. [CrossRef]
47. Hu, J.; Wang, K. Effects of Size and Uncompacted Voids of Aggregate on Mortar Flow Ability. *J. Adv. Concr. Technol.* **2007**, *5*, 75–85. [CrossRef]
48. Li, L.; Lin, C.; Chen, G.; Kwan, A.; Jiang, T. Effects of packing on compressive behaviour of recycled aggregate concrete. *Constr. Build. Mater.* **2017**, *157*, 757–777. [CrossRef]
49. Taboada, I.G.; González-Fonteboa, B.; Martínez-Abella, F.; Seara-Paz, S. Analysis of rheological behaviour of self-compacting concrete made with recycled aggregates. *Constr. Build. Mater.* **2017**, *157*, 18–25. [CrossRef]
50. Cortes, D.; Kim, H.-K.; Palomino, A.; Santamarina, J.C. Rheological and mechanical properties of mortars prepared with natural and manufactured sands. *Cem. Concr. Res.* **2008**, *38*, 1142–1147. [CrossRef]
51. Powers, T.C. *The Properties of Concrete*; Wiley & Sons: New York, NY, USA, 1968.
52. Kwan, A.; McKinley, M. Effects of limestone fines on water film thickness, paste film thickness and performance of mortar. *Powder Technol.* **2014**, *261*, 33–41. [CrossRef]
53. Bager, D.; Mette, R.; Rune, M. Rheology of self-compacting mortars- Influence of particle grading. *Nordic Concr. Res.* **2004**, *26*, 2–16.
54. Nel Quiroga, P.; Fowler, D.W. The Effects of Aggregate Characteristics on the Performance of Portland Cement Concrete. Ph.D. Thesis, The University of Texas, Austin, TX, USA, 2003.
55. Gram, A. Modelling Bingham Suspensional Flow Influence of Viscosity and Particle Properties Applicable to Cementitious Materials. Ph.D. Thesis, KTH Royal Institute of Technology, Stockholm, Sweden, 2015.
56. Rakhimov, R.; Rakhimova, N. XV International Congress on the Chemistry of Cement (ICCC 2019). *Stroit. Mater.* **2019**, *12*, 58–61. [CrossRef]